ARTICLE   OPEN

Achieving high-fidelity single-qubit gates in a strongly driven charge qubit with $1/f$ charge noise

Yuan-Chi Yang [1], S. N. Coppersmith[1] and Mark Friesen [1]

Charge qubits formed in double quantum dots represent quintessential two-level systems that enjoy both ease of control and efficient readout. Unfortunately, charge noise can cause rapid decoherence, with typical single-qubit gate fidelities falling below 90%. Here we develop analytical methods to study the evolution of strongly driven charge qubits, for general and $1/f$ charge-noise spectra. We show that special pulsing techniques can simultaneously suppress errors due to strong driving and charge noise, yielding single-qubit gates with fidelities above 99.9%. These results demonstrate that quantum dot charge qubits provide a potential route to high-fidelity quantum computation.

INTRODUCTION

Building high-quality qubits is a key objective in quantum information processing. Achieving high-fidelity gates requires both precise control and effective measures to combat decoherence arising from the environment. Semiconductor-based quantum dot charge qubits, for example, suffer from strong coupling to charge noise that causes voltage fluctuations on the control electrodes,[1–3] which has so far limited gate fidelities to below 90%.[4] To be suitable for scalable quantum computation, the fidelity must be increased to at least 99%.[5]

One strategy for achieving higher fidelities is to operate the qubits as fast as possible, for example, by driving them with strong microwaves. AC driving also mitigates decoherence, by elevating the relevant noise frequencies to the microwave regime, where their power is suppressed.[6,7] However high-power microwaves can potentially cause detrimental strong-driving effects, including Bloch–Siegert shifts of the resonant frequency[8–10] and fast oscillations superimposed on top of Rabi oscillations.[11] They can also expose the qubit to new types of decoherence such as dephasing caused by noise-induced variations of the Rabi frequency.[6,7] While Bloch–Siegert shifts can be accommodated by adjusting the driving frequency or gate time, and the induced decoherence can be suppressed by employing AC sweet spots,[12] fast oscillations may be difficult to control, resulting in gate errors. There are several known approaches for mitigating control errors, including pulse-shaping methods that suppress oscillations by engineering the pulse envelopes.[11,13,14] However, such schemes tend to increase the complexity of the control procedure.

Here we propose an alternative control scheme for strong driving, based on rectangular pulse envelopes engineered to produce nodes in the fast oscillations at the end of a gate operation, thereby minimizing their influence. We demonstrate our method on a double-quantum-dot charge qubit, showing that high-fidelity gate operations can be achieved in charge qubits under strong driving, even while $1/f$ noise is applied to the double-dot detuning parameter. This noise spectrum is particularly interesting because it has both Markovian and non-Markovian components. By employing both numerical and analytical techniques, we identify specific rotations that synchronize Rabi and fast oscillations, yielding a complete set of single-qubit gates that suppress control errors. We then propose a protocol for suppressing decoherence caused by charge noise, yielding gates with fidelities higher than 99.9%, for typical charge noise magnitudes.[1,3,15,16]

We also develop an analytical formalism based on a cumulant expansion, to accurately describe qubit dynamics in the presence of time-averaged $1/f$ noise. This formalism allows us explicitly calculate and distinguish between strong driving control errors and decoherence occurring in the weak and strong driving limits.

RESULTS

Noise-free evolution

The basis states of a double quantum dot charge qubit, $|L\rangle$ and $|R\rangle$, represent the localized positions of an excess charge in the left or right dot, as indicated in Fig. 1a.[4,17,18] We consider ac gating of a single qubit, with the Hamiltonian $\mathcal{H}_{sys} = \mathcal{H}_q + \mathcal{H}_{ac}$, where $\mathcal{H}_q = -(\varepsilon/2)\sigma_x - \Delta\sigma_z$, the σ_i are Pauli matrices, ε is the detuning parameter (defined as the energy difference between the two dots), and Δ is the tunnel coupling between the dots. Here we have expressed $\mathcal{H}_{sys}$ in the eigenbasis $\{|0\rangle = (|L\rangle - |R\rangle)/\sqrt{2}, |1\rangle = (|L\rangle + |R\rangle)/\sqrt{2}\}$, corresponding to the charge qubit "sweet spot" $\varepsilon = 0$, where it is first-order insensitive to electrical noise.[4] Unless otherwise noted, we assume that the nominal operating point is $\varepsilon = 0$ throughout the remainder of this work. When a microwave signal is applied to ε, the driving Hamiltonian is given by $\mathcal{H}_{ac} = (A_\varepsilon/2)\sigma_x\cos(\omega_d t + \phi)$, where A_ε is the driving amplitude, ω_d is its angular frequency, and ϕ is the phase at time $t = 0$, when the drive is initiated.

First, we follow ref. [11] and obtain exact solutions for strongly-driven qubits in the absence of noise, up to arbitrary order in the strong-driving parameter $\gamma = A_\varepsilon/16\Delta$. Expanding the time-evolution operator order-by-order as $U_0(t) = \sum_{n=0}^{\infty} \gamma^n U_0^{(n)}$, we

[1]Department of Physics, University of Wisconsin-Madison, Madison, WI 53706, USA
Correspondence: Yuan-Chi Yang (yang339@wisc.edu) or Mark Friesen (friesen@physics.wisc.edu)
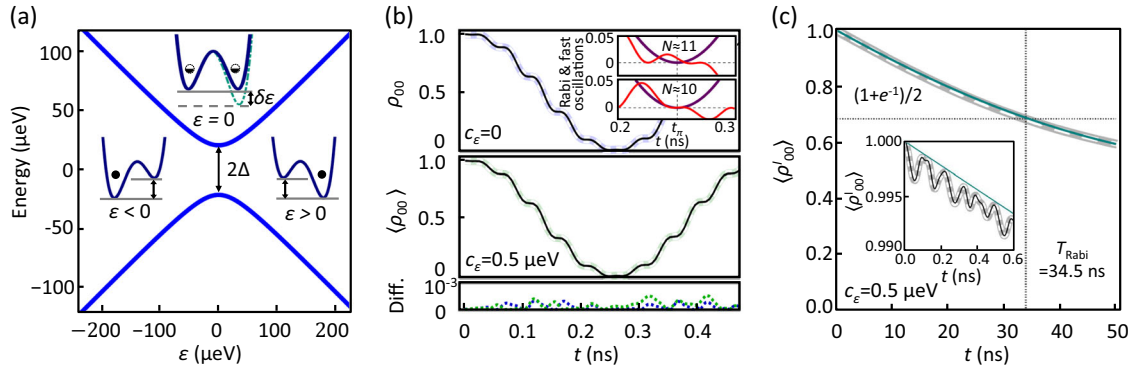
Fig. 1 Strongly driven charge qubit. **a** Energy level diagram of a charge qubit. The insets depict a double quantum dot in three regimes of detuning, ε. (A potential charge noise fluctuation is shown as a dashed line.) Here, filled circles indicate the position of the excess electron in the ground state, and the barrier between the dots induces a tunnel coupling, Δ. **b** Time evolution of the density matrix element ρ_{00} in the laboratory frame, including numerical simulations (dashed lines), analytical calculations obtained from Eq. (4) (solid black lines), and their differences (dotted lines). (Here, brackets $\langle \cdot \rangle$ denote a noise average.) In all cases, we use $\{\varepsilon, \Delta, A_\varepsilon\}/h = \{0, 5, 4\}$ GHz, $\phi = \pi/4$ and initial state $|0\rangle$. We assume the charge noise follows the $1/f$ spectrum of Eq. (3), with frequency cutoffs $\omega_l/2\pi = 0.193$ MHz and $\omega_h/2\pi = 80.8$ GHz, and noise amplitudes c_ε as indicated. The insets of **b** show blow-ups of the evolution near the end of a π-rotation ($t = t_\pi$), decomposed into their Rabi (dark purple) and fast-oscillation components (red). The oscillations are synchronized at t_π when $N = (2\theta\tilde{\omega}_{res})/(\pi\Omega)$ is an even integer, resulting in high-fidelity gates. (The main panels also use $N = 10$.) Charge noise causes a slight decay of $\langle\rho_{00}\rangle$ at the end of the simulation period ($2t_\pi \simeq 0.5$ ns), which can be observed more clearly at long times in **c**. **c** Time evolution of the density matrix element ρ'_{00} in the interaction frame, including numerical simulations (dashed gray line) and the simple asymptotic expression from Eq. (5) (solid cyan line) with corrections to K_φ up to $O[\gamma^2]$ and corrections to K_M and $K_{nMn\varphi}$ up to $O[\gamma]$, as discussed in Supplementary Sec. S3. The inset shows a short-time blow-up in the interaction frame; it further includes our full analytical calculations obtained from Eq. (4) (solid black line)

obtain

$$U_0^{(0)}(t) = \begin{pmatrix} e^{i\tilde{\omega}_{res}t}\cos(\Omega t/2) & -ie^{i(\tilde{\omega}_{res}t+\phi)}\sin(\Omega t/2) \\ -ie^{-i\phi}\sin(\Omega t/2) & \cos(\Omega t/2) \end{pmatrix}. \quad (1)$$

[Higher-order terms are provided in Supplementary Section S2, Eq. (S5)]. Here, we consider only resonant driving, $\omega_d = \tilde{\omega}_{res}$, where $\hbar\tilde{\omega}_{res} = 2\Delta(1 + 4\gamma^2)$ is the renormalized resonant angular frequency, including Bloch–Siegert corrections, and $\hbar\Omega = A_\varepsilon(1 + \gamma^2)/2$ is the renormalized Rabi angular frequency.

In the rotating frame defined by $\mathcal{H}_{rot} = U_{rot}^\dagger \mathcal{H}_{sys} U_{rot} - i\hbar U_{rot}^\dagger(d/dt)U_{rot}$, with $U_{rot} = \text{diag}[e^{i\omega_d t/2}, e^{-i\omega_d t/2}]$, the ideal evolution term $U_0^{(0)}$ generates smooth, sinusoidal, Rabi oscillations, corresponding to rotations about the $(\cos\phi, -\sin\phi, 0)$ axis of the Bloch sphere. The $U_0^{(1)}$ term represents the dominant fast oscillations associated with strong driving, with amplitude $\sim\gamma$. Both drive components can be observed in the top panel of Fig. 1b, where we show that our analytical results (shown here up to $O[\gamma^2]$) agree well with the results of numerical simulations of the full Hamiltonian.

Fast oscillations can cause gate infidelity. For example, if we consider an $R_\theta(\phi)$ rotation of angle θ about the $(\cos\phi, -\sin\phi, 0)$ axis, the fast oscillations may prevent the density matrix element ρ_{00} from reaching 0 at the end of a gate period, t_π. We see this more clearly by plotting the fast and Rabi oscillation components separately in the top inset of Fig. 1b. On the other hand, we may adjust the pulse parameters A_ε and ϕ to synchronize the fast oscillations with the slower Rabi oscillations, as shown in the bottom inset, to obtain an $R_\theta(\phi)$ gate with much higher fidelity.

We characterize the infidelity arising from the fast oscillations by computing the process fidelity $F_\theta(\phi)$, defined by comparing the ideal evolution operator $U_0^{(0)}$ to the actual evolution U_0, for $R_\theta(\phi)$ in the rotating frame. [see Eq. (S2) of Supplementary Section S1 for a precise definition of the process fidelity]. We find that specific A_ε's give rotations with perfect fidelity when $\theta = \pi, 2\pi, 3\pi, \ldots$ for any ϕ.

More importantly, when $\phi = \pi/4, 3\pi/4, 5\pi/4, \ldots$, we obtain

$$\begin{aligned} 1 - F_\theta(\phi) = 2\gamma^2[1 - \cos(2\theta\tilde{\omega}_{res}/\Omega)] \\ + 4\gamma^3 \sin\theta\sin(2\theta\tilde{\omega}_{res}/\Omega) + O[\gamma^4], \end{aligned} \quad (2)$$

where, again, $\gamma = A_\varepsilon/(16\Delta)$. For these values of ϕ, the infidelity due to strong-driving errors is bounded above by $\sim4\gamma^2$. Moreover, the oscillations are synchronized, yielding perfect fidelity (up to $O[\gamma^4]$), when $2\theta\tilde{\omega}_{res}/\Omega = N\pi$, with N an even integer. Since this condition can be met for a continuous range of θ by adjusting Ω (i.e., A_ε), and since $\phi = \pi/4$ and $3\pi/4$ represent orthogonal rotation axes, the rotations $\{R_\theta(\pi/4), R_\theta(3\pi/4)\}$ therefore generate a complete set of high-fidelity single-qubit gates. Additional phase control is provided by adjusting the waiting time between ac pulses. Unless otherwise noted, we set $\phi = \pi/4$ for the remainder of our analysis.

Charge noise
We introduce charge noise into our analysis through the Hamiltonian term $\mathcal{H}_n = h_n\delta\varepsilon(t)$, where $\delta\varepsilon(t)$ is a random variable affecting the detuning parameter and $h_n = -\sigma_x/2$ is referred to as the noise matrix.[1,3,15,16] The noise is characterized in terms of its time correlation function $S(t_1 - t_2) = \langle\delta\varepsilon(t_1)\delta\varepsilon(t_2)\rangle$, where the brackets denote an average over noise realizations, and the corresponding noise power spectrum is $\tilde{S}(\omega) = \int_{-\infty}^{\infty} dt\, e^{i\omega t}S(t)$.[19] Although we obtain analytical solutions for generic noise spectra in Supplementary Sec. S3, below we focus on $1/f$ noise, including in our simulations, due to its relevance for charge noise in semiconducting devices:[20,21]

$$\tilde{S}(\omega) = \begin{cases} c_\varepsilon^2 \frac{2\pi}{|\omega|} & (\omega_l \le |\omega| \le \omega_h) \\ 0 & (\text{otherwise}) \end{cases}, \quad (3)$$

where c_ε is related to the standard deviation of the detuning noise, σ_ε, via $\sigma_\varepsilon = c_\varepsilon[2\ln(\sqrt{2\pi}c_\varepsilon/\hbar\omega_l)]^{1/2}$,[6,22] and ω_l (ω_h) are low (high) cutoff angular frequencies. We note that all frequencies relevant for qubit operation occur between these two cutoffs, so that the decoherence includes both Markovian and non-Markovain contributions.

We now present numerical simulations of a strongly driven, noisy charge qubit. A typical result is shown in the middle panel of Fig. 1b, where the suppression of Rabi oscillations is a direct consequence of the charge noise. To differentiate the effects of decoherence from those arising from strong driving, we present the same results in an interaction frame defined by U_0, $\rho^I = U_0^\dagger \rho U_0$, in which the fast oscillations due to strong driving are not observed. Figure 1c shows the resulting long-time decay of the density matrix, while the inset shows the short-time behavior on an expanded scale. Note that the fast oscillations observed here do not arise directly from strong driving, but rather from non-Markovian noise terms, as discussed below.

Analytical solutions, with charge noise

Several theoretical techniques have been applied to noisy, driven two-level systems, including master equations,[6,7,23–27] dissipative Lander-Zener-Stückelberg interferometry,[28,29] and treatments of spin-Boson systems.[30–32] In Supplementary Sec. S3, we solve the dynamical equation in the interaction frame via a cumulant expansion,[33,34] truncated at $O[(\delta\varepsilon/\hbar\Omega)^2]$. The time evolution can be written in the form $\mathbf{r}^I(t) = \exp[K(t)]\mathbf{r}^I(0)$ by expressing $\langle\rho^I\rangle = 1/2\left(I_2 + r_x^I\sigma_x + r_y^I\sigma_y + r_z^I\sigma_z\right)$. Here, I_2 is the 2×2 identity matrix, $\mathbf{r}^I = \left(r_x^I, r_y^I, r_z^I\right)$ is the Bloch vector, and $K(t)$ is a 3×3 evolution matrix, given by

$$[K(t)]_{ij} = -\frac{4}{\hbar^2}\sum_{\omega_1,\omega_2}\left[-a_{j,\omega_1}a_{i,\omega_2} + \delta_{ij}\sum_{k=1}^{3}a_{k,\omega_1}a_{k,\omega_2}\right]I(t,\omega_1,\omega_2),$$

(4)

where we have expand the noise matrix in the interaction frame into Fourier components $h_n^I(t) \equiv U_0^\dagger h_n U_0 = \sum_{i,\omega}a_{i,\omega}e^{i\omega t}$, and defined $I(t,\omega_1,\omega_2) \equiv \int_0^t dt_1\int_0^{t_1}dt_2 e^{i\omega_1 t_1}e^{i\omega_2 t_2}S(t_1 - t_2)$. Since U_0 can be expressed order-by-order in γ, the same is also true of $a_{i,\omega}$, allowing us to distinguish the effects arising in the weak-drive limit, $O[\gamma^0]$, from the strong-driving limit, $O[\gamma^n]$, for $n \geq 1$. The accuracy of this cumulant approach is evident in Fig. 1b, c, where the theoretical results (solid black line) are seen to capture all the fine structure of the simulations. Indeed, the bottom panel of Fig. 1b indicates that the analytical and numerical solutions differ by $<10^{-3}$ over the entire range plotted.

The physics of noise-averaged qubit dynamics is encoded in $K(t)$, which can be decomposed into a sum of Markovian terms K_M, and non-Markovian terms. The latter may be further divided into pure-dephasing terms K_φ,[26,35,36] and non-Markovian-non-dephasing terms $K_{nMn\varphi}$. Pure-dephasing terms are conventionally associated with the integral $I(t, \omega_1 = 0, \omega_2 = 0) \sim t^2 \ln(1/\omega_l t)$.[26,35,36] However, since K is defined in a rotating frame, "pure dephasing" has a different meaning than in the laboratory frame:[7,26] here, the leading order contributions to K_φ are proportional to γ^2, and are therefore attributed to strong driving. Markovian terms are associated with the integral $\text{Re}[I(t, \omega, -\omega)]$, corresponding to short correlation times [see Supplementary Eq. (S34)], and exponential decay ($\sim e^{-\Gamma t}$). The dominant non-Markovian-non-dephasing terms are associated with the integral $\text{Im}[I(t, \omega, -\omega)]$, yielding slow oscillations in the rotating frame, as well as the fast oscillations in the inset of Fig. 1c. Since it is common in the literature to treat the dephasing and depolarizing channels separately,[26] it is significant that our method encompasses both phenomena (and other behavior, including $K_{nMn\varphi}$) within a common framework, allowing us to compare and contrast their effects.

Asymptotic solutions

We can compute the asymptotic behavior of $\mathbf{r}^I(t)$ analytically, using the cumulant expansion. In the limit $t \gg 1/\omega$, where ω is any
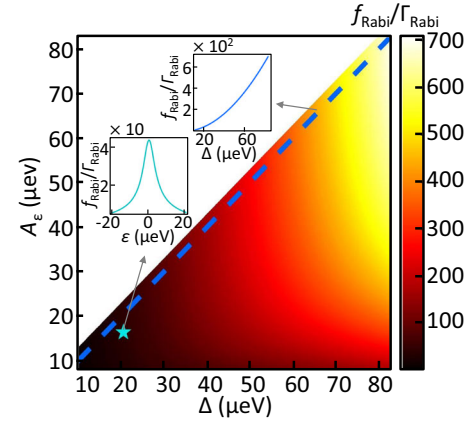

Fig. 2 Figure of merit (FOM) of gates of a strongly driven charge qubit. Analytical calculations of the FOM f_{Rabi}/Γ_{Rabi} of a strongly driven charge qubit, as a function of the tunnel coupling Δ and driving amplitude A_ε, at $\varepsilon = 0$ and $\phi = \pi/4$, based on the asymptotic formula in Eq. (5), with corrections to K_φ up to $O[\gamma^2]$ and corrections to K_M and $K_{nMn\varphi}$ up to $O[\gamma]$, as discussed in Supplementary Sec. S3. Here, f_{Rabi} is the Rabi frequency, Γ_{Rabi} is the Rabi decay rate, and the $1/f$ noise spectrum is given in Eq. (3), with $c_\varepsilon = 0.5$ μeV, $\omega_l/2\pi = 1$ Hz, and $\omega_h/2\pi = 100$ THz. The upper inset shows a line-cut along $A_\varepsilon = \Delta$ in the main figure (blue dashed line), revealing a FOM as high as 700. In the lower inset, we fix $\Delta/h = 5$ GHz and $A_\varepsilon/h = 4$ GHz (cyan star), but allow ε to vary, confirming that the FOM is maximized at the sweet spot, $\varepsilon = 0$, where the qubit is first-order insensitive to detuning noise

characteristic qubit frequency, many terms drop out, yielding the leading-order solution in γ:

$$\mathbf{r}^I(t) = \frac{e^{-\Gamma_z t}}{\sqrt{2}}\left[\sin(\Gamma_{nMn\varphi}t), \sin(\Gamma_{nMn\varphi}t), \sqrt{2}\cos(\Gamma_{nMn\varphi}t)\right],$$

(5)

for the initial state $|0\rangle$. Here, the decoherence is dominated by the integral $I(t, \omega, -\omega) \approx \tilde{S}(\omega)t/2 + \tilde{S}_{imag}(\omega)t$, whose imaginary part is given by $\tilde{S}_{imag}(\omega) \equiv c_\varepsilon^2(2i/\omega)\ln|\omega/\omega_l|$. The real part describes exponential decay, giving the Markovian decoherence rate for driven evolution, $\Gamma_z = (1/16\hbar^2)\left[4\tilde{S}(\tilde{\omega}_{res}) + \tilde{S}(\tilde{\omega}_{res} + \Omega) + \tilde{S}(\tilde{\omega}_{res} - \Omega)\right]$ as observed in Fig. 1c, which can also be derived from Bloch-Redfield theory.[26,27] The imaginary part corresponds to a non-Markovian-non-dephasing noise-induced rotation with frequency $\Gamma_{nMn\varphi} = (-i/8\hbar^2)\left[(\tilde{S}_{imag}(-\tilde{\omega}_{res} + \Omega) + \tilde{S}_{imag}(\tilde{\omega}_{res} + \Omega))\right]$, originating from the integrated low-frequency ("quasistatic") portion of the noise spectrum, $\left[\int_{\omega_l}^{\omega}d\omega' S(\omega')/\pi\right]^{1/2} = c_\varepsilon[2\ln(\omega/\omega_l)]^{1/2}$. Besides these lowest-order results, which are the only important terms under weak driving, we can also compute higher-order corrections to these terms that become important under strong driving. Such high-order results are presented in Supplementary Section S3.

We can define a figure of merit (FOM), f_{Rabi}/Γ_{Rabi}, corresponding to the number of coherent $R_{2\pi}(\pi/4)$ rotations within a Rabi decay period $T_{Rabi} = 1/\Gamma_{Rabi}$ (not including strong-driving control errors), where the Rabi decay rate Γ_{Rabi} is determined from Eq. (5) such that $\langle\rho_{00}^I(t = 1/\Gamma_{Rabi})\rangle \equiv (1 + e^{-1})/2$. By exploring a range of control parameters in Fig. 2, we first confirm that the FOM is strongly enhanced at the sweet spot $\varepsilon = 0$ (lower inset). Increasing the tunnel coupling Δ and the driving amplitude A_ε both enhance the FOM, as shown in the main panel. By increasing Δ and A_ε simultaneously, as shown in the upper inset, we find that the FOM can exceed 700 for a physically realistic charge noise amplitude of $c_\varepsilon = 0.5$ μeV ($\sigma_\varepsilon = 3.12$ μeV).[1,3,15,16]
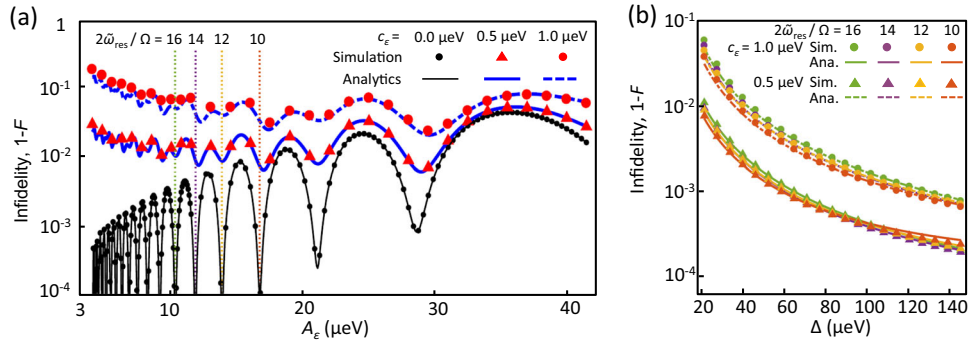
Fig. 3 Characterization of the fidelity. Dependence of the infidelity $1 - F_\pi(\pi/4)$ of a strongly driven charge qubit on **a** the driving amplitude A_ε, with $\Delta/h = 5$ GHz, and on **b** the tunnel coupling Δ, with $N = (2\theta\tilde{\omega}_{res})/(\pi\Omega) = 10, 12, 14, 16$ held constant. Here, $\varepsilon = 0$, and the charge noise is given by Eq. (3), with $\omega_l/2\pi = 1$ Hz, $\omega_h/2\pi = 256$ GHz, and the values of c_ε are indicated. Note that low frequencies (<0.3 MHz) are approximated as quasistatic in these simulations, while the analytical results are obtained from Eq. (4), up to $O[\gamma^3]$ [or $O[\gamma^4]$ for $c_\varepsilon = 0$, see Supplementary Eq. (S12)]. In **b**, the infidelities are computed at the "dips" indicated in **a**

$R_\pi(\pi/4)$ gate fidelity

We now compute process fidelities for $R_\pi(\pi/4)$ gates, using the χ-matrix method described in Supplementary Sec. S1. Control errors due to strong driving are investigated by considering $U_0^{(0)}$ as the ideal evolution. The results of both numerical and analytical calculations are shown in Fig. 3. For no noise ($c_\varepsilon = 0$), the simulations are essentially identical to Eq. (2), revealing "dips" of low infidelity, enabled by synchronized oscillations. For $\phi = \pi/4$, the dip minima are proportional to γ^4, while their widths are proportional to γ^2 [see Supplementary Eq. (S13)], suggesting potential benefits of working at large $A_\varepsilon \propto \gamma$. As c_ε increases, the infidelity also grows, including both Markovian (K_M), and non-Markovian contributions (K_φ and $K_{nMn\varphi}$). Initially, the envelope of the infidelity oscillations decreases with A_ε, because fast gates have less time to be affected by noise; it then increases, due to the combination of strong-driving effects and the decoherence induced by strong driving. For smaller A_ε, the simulations deviate slightly from the analytical results when the high-order noise terms become non-negligible. In all cases, the infidelity is locally minimized when A_ε is positioned at a dip.

For the noise levels considered in Fig. 3a, which are consistent with recent experiments,[1,3,15,16] we obtain $F_{max} \lesssim 99\%$, which is insufficient for achieving high-fidelity gates. However, the following procedure can be used to suppress both control errors and decoherence. First, A_ε is tuned to a dip. Then, Δ and A_ε are simultaneously increased while holding $\gamma = A_\varepsilon/16\Delta$ (and thus N) fixed. In this way, we remain in a dip, while increasing the gate speed to suppress noise effects. The results are shown in Fig. 3b. Here, when $c_\varepsilon = 1$ μeV ($\sigma_\varepsilon = 6.36$ μeV), we obtain fidelities >99% when $\Delta > 40$ μeV, and >99.9% when $\Delta > 120$ μeV. The corresponding qubit frequencies, $2\Delta/h = 29.3$ GHz and 58.0 GHz, are comparable to the qubit frequency of the quantum dot spin qubit in ref. [37], and the Rabi frequencies $\simeq 4\Delta/hN$ are generally lower. We note that this protocol is applicable for any rotation angle θ, as shown in Supplementary Section S5.

DISCUSSION

We have developed a new scheme for effectively harnessing strong driving to perform high-fidelity gates in quantum double-dot charge qubits, even in the presence of realistic 1/f noise. Our protocol, and our analytical formalism, are both applicable to other solid-state systems, including superconducting flux qubits[38,39] and quantum-dot singlet-triplet qubits,[15,40,41] and can be extended to systems with multiple levels, including quantum-

dot hybrid qubits[3,11,42–46] and charge-quadrupole qubits.[47,48] Phonon-induced decoherence can be also analyzed in this formalism, after first averaging the phonons over the corresponding thermal distribution.[34,49–51] However, the effectiveness of the protocol may be reduced compared to case of charge noise, since the power spectral density of phonons typically increases with the frequency.

A possible challenge for implementing this proposal is the requirement of large tunnel couplings, which could results in fast qubits that are difficult to control. However, by employing high-order synchronized oscillations (e.g. $N \sim 10$), we can reduce gate speeds to be compatible with current experiments. Improvements in ac control technology and materials with lower charge noise can also mitigate the technical challenges. On the other hand, the phonon-induced relaxation rate increases strongly with tunnel coupling,[52–54] which will set an upper bound on the qubit coherence. Moving forward, we note that the phase, ϕ, represents an important control knob in our proposal, and can be viewed as a simple pulse-shaping tool. In future work, it should be possible to combine the methods described here with conventional pulse shaping techniques, which would be expected to further improve the gate fidelities.[11,13,14]

METHODS

Numerical Simulation

We numerically simulate the Schrodinger equation of a strongly driven, noisy charge qubit, $i\hbar d\rho/dt = [\mathcal{H}_{sys} + \mathcal{H}_n, \rho]$, where the time sequences for $\delta\varepsilon(t)$ are obtained by generating a white noise sequence, then scaling its Fourier transform by an appropriate spectral function,[55] such as Eq. (3). We then average the density matrix $\langle\rho(t)\rangle$ over noise realizations. Details of these procedures are provided in Supplementary Sec. S4.

Analytical formalism

We analytically solve the dynamical equation $i\hbar d\rho^I/dt = \delta\varepsilon(t)\mathcal{L}\rho^I$ in the interaction frame, where $\mathcal{L}\rho^I \equiv [h_n^I, \rho^I]$ and $h_n^I = U_0^\dagger h_n U_0$. We then average over the noise via a cumulant expansion,[33,34] truncated at $O[(\delta\varepsilon/\hbar\Omega)^2]$, yielding $\langle\rho^I(t)\rangle = \exp\left[-\frac{1}{\hbar^2}\int_0^t dt_1 \int_0^{t_1} dt_2 \mathcal{L}(t_1)\mathcal{L}(t_2)S(t_1 - t_2)\right]\rho^I(0)$, where we have assumed that the noise is stationary, with zero mean ($\langle\delta\varepsilon\rangle = 0$). Details of the calculations are provided in Supplementary Sec. S3.

DATA AVAILABILITY

The data and numerical codes that support the findings of this study are available from the corresponding author upon reasonable request.

AUTHOR CONTRIBUTIONS

Y.Y. performed numerical simulations and analytical calculations. Y.Y., S.N.C., and M.F. analyzed the results and prepared the manuscript. Work was carried out under supervison of S.N.C. and M.F.

ADDITIONAL INFORMATION

Supplementary information accompanies the paper on the *npj Quantum Information* website (https://doi.org/10.1038/s41534-019-0127-1).

Competing interests: The authors declare no competing interests.

Publisher's note: Springer Nature remains neutral with regard to jurisdictional claims in published maps and institutional affiliations.

REFERENCES

1. Petersson, K. D., Petta, J. R., Lu, H. & Gossard, A. C. Quantum coherence in a one-electron semiconductor charge qubit. *Phys. Rev. Lett.* **105**, 246804 (2010).
2. Dial, O. E. et al. Charge noise spectroscopy using coherent exchange oscillations in a singlet-triplet qubit. *Phys. Rev. Lett.* **110**, 146804 (2013).
3. Thorgrimsson, B. et al. Extending the coherence of a quantum dot hybrid qubit. *npj Quantum Inf.* **3**, 32 (2017).
4. Kim, D. et al. Microwave-driven coherent operation of a semiconductor quantum dot charge qubit. *Nat. Nano.* **10**, 243 (2015).
5. Fowler, A. G., Mariantoni, M., Martinis, J. M. & Cleland, A. N. Surface codes: Towards practical large-scale quantum computation. *Phys. Rev. A.* **86**, 032324 (2012).
6. Wong, C. H. High-fidelity ac gate operations of a three-electron double quantum dot qubit. *Phys. Rev. B* **93**, 035409 (2016).
7. Yan, F. et al. Rotating-frame relaxation as a noise spectrum analyser of a superconducting qubit undergoing driven evolution. *Nat. Commun.* **4**, 2337 (2013).
8. Bloch, F. & Siegert, A. Magnetic resonance for nonrotating fields. *Phys. Rev.* **57**, 522–527 (1940).
9. Shirley, J. H. Solution of the Schrödinger equation with a hamiltonian periodic in time. *Phys. Rev.* **138**, B979–B987 (1965).
10. Romhányi, J., Burkard, G. & Pályi, A. Subharmonic transitions and Bloch-Siegert shift in electrically driven spin resonance. *Phys. Rev. B* **92**, 054422 (2015).
11. Yang, Y.-C., Coppersmith, S. N. & Friesen, M. Achieving high-fidelity single-qubit gates in a strongly driven silicon-quantum-dot hybrid qubit. *Phys. Rev. A.* **95**, 062321 (2017).
12. Didier, N., Sete, E. A., Combes, J. & da Silva, M. P. Ac flux sweet spots in parametrically-modulated superconducting qubits. Preprint at https://arxiv.org/abs/1807.01310.
13. Motzoi, F., Gambetta, J. M., Rebentrost, P. & Wilhelm, F. K. Simple pulses for elimination of leakage in weakly nonlinear qubits. *Phys. Rev. Lett.* **103**, 110501 (2009).
14. Motzoi, F. & Wilhelm, F. K. Improving frequency selection of driven pulses using derivative-based transition suppression. *Phys. Rev. A.* **88**, 062318 (2013).
15. Wu, X. et al. Two-axis control of a singlet-triplet qubit with an integrated micromagnet. *Proc. Natl Acad. Sci. USA* **111**, 11938–11942 (2014).
16. Shi, Z. et al. Coherent quantum oscillations and echo measurements of a Si charge qubit. *Phys. Rev. B* **88**, 075416 (2013).
17. Hayashi, T., Fujisawa, T., Cheong, H. D., Jeong, Y. H. & Hirayama, Y. Coherent manipulation of electronic states in a double quantum dot. *Phys. Rev. Lett.* **91**, 226804 (2003).
18. Gorman, J., Hasko, D. G. & Williams, D. A. Charge-qubit operation of an isolated double quantum dot. *Phys. Rev. Lett.* **95**, 090502 (2005).
19. Clerk, A. A., Devoret, M. H., Girvin, S. M., Marquardt, F. & Schoelkopf, R. J. Introduction to quantum noise, measurement, and amplification. *Rev. Mod. Phys.* **82**, 1155–1208 (2010).
20. Kuhlmann, A. V. et al. Charge noise and spin noise in a semiconductor quantum device. *Nat. Phys.* **9**, 570 (2013).
21. Paladino, E., Galperin, Y. M., Falci, G. & Altshuler, B. L. 1/f noise: Implications for solid-state quantum information. *Rev. Mod. Phys.* **86**, 361–418 (2014).
22. Makhlin, Y., Schön, G. & Shnirman, A. Dissipative effects in Josephson qubits. *Chem. Phys.* **296**, 315–324 (2004).
23. Geva, E., Kosloff, R. & Skinner, J. L. On the relaxation of a two-level system driven by a strong electromagnetic field. *J. Chem. Phys.* **102**, 8541–8561 (1995).
24. Smirnov, A. Y. Decoherence and relaxation of a quantum bit in the presence of Rabi oscillations. *Phys. Rev. B* **67**, 155104 (2003).
25. Jing, J., Huang, P. & Hu, X. Decoherence of an electrically driven spin qubit. *Phys. Rev. A.* **90**, 022118 (2014).
26. Ithier, G. et al. Decoherence in a superconducting quantum bit circuit. *Phys. Rev. B* **72**, 134519 (2005).
27. Slichter, C. *Principles of Magnetic Resonance* (Springer, Berlin, 1990).
28. Shevchenko, S., Ashhab, S. & Nori, F. Landau-Zener-Stückelberg interferometry. *Phys. Rep.* **492**, 1–30 (2010).
29. Ferrón, A., Domínguez, D. & Sánchez, M. J. Dynamic transition in Landau-Zener-Stückelberg interferometry of dissipative systems: the case of the flux qubit. *Phys. Rev. B* **93**, 064521 (2016).
30. Goorden, M. C., Thorwart, M. & Grifoni, M. Spectroscopy of a driven solid-state qubit coupled to a structured environment. *Eur. Phys. J. B* **45**, 405–417 (2005).
31. Grifoni, M. & Hänggi, P. Driven quantum tunneling. *Phys. Rep.* **304**, 229–354 (1998).
32. Hartmann, L., Goychuk, I., Grifoni, M. & Hänggi, P. Driven tunneling dynamics: Bloch-Redfield theory versus path-integral approach. *Phys. Rev. E* **61**, R4687–R4690 (2000).
33. Kubo, R. Generalized cumulant expansion method. *J. Phys. Soc. Jpn.* **17**, 1100–1120 (1962).
34. Kubo, R. Stochastic Liouville equations. *J. Math. Phys.* **4**, 174–183 (1963).
35. Paladino, E., Faoro, L., Falci, G. & Fazio, R. Decoherence and 1/f noise in Josephson qubits. *Phys. Rev. Lett.* **88**, 228304 (2002).
36. Astafiev, O., Pashkin, Y. A., Nakamura, Y., Yamamoto, T. & Tsai, J. S. Quantum noise in the Josephson charge qubit. *Phys. Rev. Lett.* **93**, 267007 (2004).
37. Chan, K. W. et al. Assessment of a silicon quantum dot spin qubit environment via noise spectroscopy. *Phys. Rev. Appl.* **10**, 044017 (2018).
38. Deng, C., Orgiazzi, J.-L., Shen, F., Ashhab, S. & Lupascu, A. Observation of Floquet states in a strongly driven artificial atom. *Phys. Rev. Lett.* **115**, 133601 (2015).
39. Deng, C., Shen, F., Ashhab, S. & Lupascu, A. Dynamics of a two-level system under strong driving: Quantum-gate optimization based on Floquet theory. *Phys. Rev. A.* **94**, 032323 (2016).
40. Nichol, J. M. et al. High-fidelity entangling gate for double-quantum-dot spin qubits. *npj Quantum Inf.* **3**, 3 (2017).
41. Culcer, D. & Zimmerman, N. M. Dephasing of Si singlet-triplet qubits due to charge and spin defects. *Appl. Phys. Lett.* **102**, 232108 (2013).
42. Shi, Z. et al. Fast hybrid silicon double-quantum-dot qubit. *Phys. Rev. Lett.* **108**, 140503 (2012).
43. Koh, T. S., Gamble, J. K., Friesen, M., Eriksson, M. A. & Coppersmith, S. N. Pulse-gated quantum-dot hybrid qubit. *Phys. Rev. Lett.* **109**, 250503 (2012).
44. Kim, D. et al. Quantum control and process tomography of a semiconductor quantum dot hybrid qubit. *Nature* **511**, 70–74 (2014).
45. Ferraro, E., De Michielis, M., Mazzeo, G., Fanciulli, M. & Prati, E. Effective Hamiltonian for the hybrid double quantum dot qubit. *Quantum Inf. Process.* **13**, 1155–1173 (2014).
46. Cao, G. et al. Tunable hybrid qubit in a GaAs double quantum dot. *Phys. Rev. Lett.* **116**, 086801 (2016).
47. Friesen, M., Ghosh, J., Eriksson, M. A. & Coppersmith, S. N. A decoherence-free subspace in a charge quadrupole qubit. *Nat. Commun.* **8**, 15923 (2017).
48. Ghosh, J., Coppersmith, S. N. & Friesen, M. Pulse sequences for suppressing leakage in single-qubit gate operations. *Phys. Rev. B* **95**, 241307 (2017).
49. Kornich, V., Kloeffel, C. & Loss, D. Phonon-mediated decay of singlet-triplet qubits in double quantum dots. *Phys. Rev. B* **89**, 085410 (2014).
50. Kornich, V., Kloeffel, C. & Loss, D. Phonon-assisted relaxation and decoherence of singlet-triplet qubits in Si/SiGe quantum dots. *Quantum* **2**, 70 (2018).
51. Kornich, V., Vavilov, M. G., Friesen, M. & Coppersmith, S. N. Phonon-induced decoherence of a charge quadrupole qubit. *New J. Phys.* **20**, 103048 (2018).
52. Wang, K., Payette, C., Dovzhenko, Y., Deelman, P. W. & Petta, J. R. Charge relaxation in a single-electron Si/SiGe double quantum dot. *Phys. Rev. Lett.* **111**, 046801 (2013).
53. Stace, T. M., Doherty, A. C. & Barrett, S. D. Population inversion of a driven two-level system in a structureless bath. *Phys. Rev. Lett.* **95**, 106801 (2005).

54. Colless, J. I. et al. Raman phonon emission in a driven double quantum dot. *Nat. Commun.* **5**, 3716 (2014).
55. Kawakami, E. et al. Gate fidelity and coherence of an electron spin in an Si/SiGe quantum dot with micromagnet. *Proc. Natl Acad. Sci. USA* **113**, 11738–11743 (2016).